Available online at www.sciencedirect.com
SCIENCE DIRECT®
Journal of Magnetic Resonance 171 (2004) 244–252
JMR Journal of Magnetic Resonance
www.elsevier.com/locate/jmr

Separation and characterization of different signals from intermolecular three-spin orders in solution NMR

Zhong Chen[a,b,*], Zhi-Wei Chen[a], Dennis W. Hwang[b], Jianhui Zhong[c], Lian-Pin Hwang[b]

[a] *Departments of Physics and Chemistry, Xiamen University, and State Key Laboratory of Physical Chemistry of Solid Surface, Xiamen, Fujian 361005, PR China*
[b] *Department of Chemistry, National Taiwan University, and Institute of Atomic and Molecular Science, Academia Sinica, Taipei, Taiwan, ROC*
[c] *Departments of Radiology and Physics and Astronomy, University of Rochester, Rochester, NY 14642, USA*

Received 18 September 2003; revised 30 August 2004
Available online 25 September 2004

Abstract

In this paper, signals originating from a pure specific coherence of intermolecular three-spin orders were separated and characterized experimentally in highly polarized two-component spin systems. A modified CRAZED sequence with selective radio-frequency excitation was designed to separate the small signals from the strong conventional single-spin single-quantum signals. General theoretical expressions of the pulse sequence with arbitrary flip angle pulses were derived using dipolar field treatment. The expressions were used to predict the relaxation and diffusion properties and optimal experimental parameters such as flip angles. For the first time, relaxation and diffusion properties of pure intermolecular single-quantum, double-quantum, and triple-quantum coherences of three-spin orders were characterized and analyzed in one-dimensional experiments. All experimental observations are in excellent agreement with the theoretical predictions. The theoretical results show that the quantum-mechanical treatment leads to exactly the same predictions as the dipolar field treatment. The quantitative study of intermolecular multiple-quantum coherences of three-spin orders presented herein provides a better understanding of their mechanisms.

Keywords: Intermolecular dipolar interactions; Multiple-quantum coherences; Three-spin order; Diffusion; Relaxation

1. Introduction

Intermolecular multiple-quantum coherence (iMQC) is a very important and versatile tool in NMR studies. For samples of concentrated solutions and with large gyromagnetic ratios in high magnetic field, multiple-spin echoes (MSEs) [1–3] or iMQCs [4,5] are usually generated by COSY revamped by asymmetric z-gradient echo detection (CRAZED) sequence, consisting of two radio-frequency (RF) pulses in combination with pulsed-field gradients (PFGs). When the ratio of the PFG areas (amplitude-duration product) before and after the second RF pulse in the CRAZED sequence is 1:n, iMQCs or MSEs of order n are observed [4]. Lee et al. [5] and Jeener [6] pointed out that MSEs and iMQCs originate from the dipolar field representing the collective distant dipolar coupling among the dipoles of the spin ensemble. Although effects originating from higher-spin terms are readily observable at high fields, most of the iMQC applications have used intermolecular zero-quantum and double-quantum coherences (iZQCs and iDQCs), which originate from the two-spin terms in equilibrium density matrix and produce the largest signals in most common cases [7–18]. Recently, we demonstrated theoretically and experimentally that the intermolecular single-quantum coherence (iSQC) signals originating from the two-spin terms are selectively excited in a two-component sample with high efficiency, which have the same

* Corresponding author. Fax: +86 592 2188054.
E-mail address: Chenz@jingxian.xmu.edu.cn (Z. Chen).

1090-7807/$ - see front matter © 2004 Elsevier Inc. All rights reserved.
doi:10.1016/j.jmr.2004.08.023

amplitude as those from iDQCs and iZQCs [19]. However, the yields of high-order coherences become inevitably low due to the hierarchical generation of iMQC. There are only a few papers to discuss triple- and higher-quantum CRAZED experiments. Ahn et al. [20] employed three ($\pi/2$) pulses in separated time intervals and phase cycling to choose signals from a specific iMQC. There are different transfer pathways during the time interval between the second and the third pulses. Since dipolar fields may be created by the second and the third pulses, respectively, it is difficult to describe the evolution behavior of the magnetization. Ardelean et al. [21,22] discussed single-quantum filter from homonuclear three-spin terms (i.e., third-order spin interactions) in Hahn echo sequence. Recently, Warren et al. [23] investigated the iSQC signals from homonuclear intermolecular longitudinal three-spin orders, including relaxation and molecular diffusion in theoretical analyses and computer simulations. Since the signals from three-spin interactions are usually much smaller than those from two-spin interactions, it is difficult to separate "pure" iSQCs signals of intermolecular three-spin orders from the much stronger conventional SQCs in homonuclear experiments. To the best of our knowledge, in the work published to date, some important issues such as how to separate "pure" iSQC signals from three-spin orders and how to characterize their relaxation and diffusion properties experimentally, have not been resolved yet. Therefore, complete theoretical expressions and quantitatively experimental characterizations are of fundamental importance for our understanding of their physical mechanisms.

Warren et al. [24] demonstrated that the excitation efficiency of conventional multiple-quantum coherences is improved by increasing selectivity. Our recent works [19,25] showed that selective excitation CRAZED sequence with a two-component sample may provide a method to resolve the problem mentioned above. In this paper, we extend the selective excitation techniques to separate and characterize different NMR signals from intermolecular three-spin orders that have not been quantified previously. A pulse sequence was designed in such a way that different signals from three-spin terms may be detected selectively. Thorough analyses of the pulse sequence were performed using the dipolar field and iMQC treatments, respectively. Moreover, dependence of the signals on the flip angles is measured and analyzed to verify the theoretical predictions.

2. Theoretical formalism

To quantify the signals from intermolecular three-spin orders, we first study the simple model of a homogeneous liquid mixture in which some molecules bear a single spin 1/2 of type I, and other molecules bear a single spin 1/2 of type S. Spins I and S could be protons, for instance, with different chemical shifts. To simplify the quantitative comparison of the results in our previous papers [19,25], here we follow the same notation as much possible: T_1^I and T_1^S are the longitudinal relaxation times, T_2^I and T_2^S are transverse relaxation times, and D_T^I and D_T^S are the translational self-diffusion coefficients of I and S spins in conventional SQC experiments, respectively. The pulse sequence shown in Fig. 1 was designed in order to characterize relaxation and diffusion properties of different signals from longitudinal three-spin orders, in which the RF pulses may be hard or Gaussian soft pulses. Small intermolecular nuclear Overhauser effects are ignored, and radiation damping effects are effectively suppressed using gradients immediately following the α and β RF pulses and detuning of the probe [25]. The desired coherence order is selected by choosing the relative area n of the gradient (with horizontal shade) immediately after the β RF pulse with respect to the one before. The magnitude G and duration δ_2 of these gradients during a given evolution period τ is kept constant to maintain a fixed dipolar correlation distance, $d = \pi/(\gamma G \delta_2)$, in which γ is the gyromagnetic ratio [5]. Since the sample dimension in our experiments is much larger than the dipolar correlation distance d, effects of sample shape can be neglected [3]. The first two gradients with the magnitude G_1 and duration δ_1 (with vertical shade) form an "active" diffusion weighting module, which allows the diffusion process during the evolution period to be investigated quantitatively [26,27]. Therefore, diffusion weighting factor is adjusted by incorporating only the parameter G_1 as a variable, which causes attenuation of signal only due to diffusion. Two different frequency offsets were used in the combined DANTE selective pulse to control the selective pre-saturation irradiation of two resonance peaks from I and S spins. The longitudinal relaxation process is probed by incorporating the saturation recovery time Δ as a variable [28]. To simplify the discussion, the spectrometer frequency is set to coincide with the resonance frequency of I spin (in absence of dipolar field shift) so

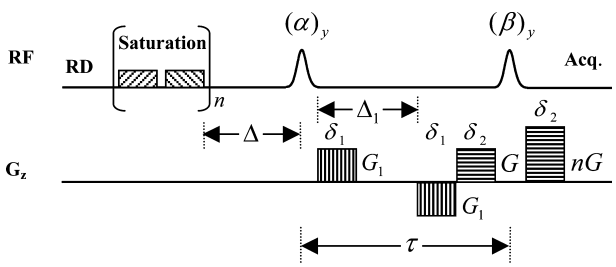

Fig. 1. A modified CRAZED sequence for detection of iMQC signals from longitudinal three-spin orders. Full vertical bars stand for RF pulses, and dash rectangles stand for gradient pulses. The first RF pulse is selectively pre-saturating for I or S spins, or both. Other experimental parameters are defined in the text.

that we only need to deal with the resonance frequency offset ω_S of S spin in the rotating frame. M_0^I and M_0^S are the equilibrium magnetization densities of the I and S spins, respectively. The I and S spins are first saturated by the appropriate pre-saturating RF pulses, then relaxation acts during the time interval Δ.

2.1. Dipolar field treatment

The dipolar field treatment provides simple expressions for uniformly modulated magnetization [3], so it is first employed to analyze the modified CRAZED sequences. For simplicity, we restrict ourselves to the treatment of dipolar field effects arising solely from coherence evolution in the t_2 interval. The following discussion will be limited to the case: (1) the dipolar correlation distance d is much smaller than the sample size; (2) the gradients are along the direction of the external magnetic field (B_0); and (3) the frequency offset $\omega_S/2\pi$ in unperturbed NMR frequency is much larger than the precession frequency due to the maximum dipolar field alone, $|\omega_S| \gg |\mu_0\gamma M_0^I|$, in which μ_0 is the magnetic permeability constant.

When the $(\alpha)_y$ RF pulse is non-selective and the $(\beta)_y$ pulse is selective to the I spin (see Fig. 1), the resulting signal with a quadrature detection scheme is described by Eq. (16) in [25]:

$$\begin{aligned} M_+^{\text{total}}(\Delta+\tau+t_2) = {} & M_0^I \mathrm{i}^{-(n+1)} \left\{ \frac{nJ_n(\xi)}{\xi} - 0.5[J_{n-1}(\xi) \right. \\ & \left. - J_{n+1}(\xi)] \cos\beta \right\} \sin\alpha (1-\mathrm{e}^{-\Delta/T_1^I}) \\ & \times \mathrm{e}^{-(\tau+t_2)/T_2^I} \mathrm{e}^{-(b_1+b_2+b_3)D_T^I} + M_0^I \mathrm{i}^{-n+1} \\ & \times J_n(\xi) \sin\beta [\cos\alpha \mathrm{e}^{-\tau/T_1^I}(1-\mathrm{e}^{-\Delta/T_1^I}) \\ & + (1-\mathrm{e}^{-\tau/T_1^I})] \mathrm{e}^{-t_2/T_2^I} \mathrm{e}^{-b_4 D_T^I} + M_0^S \mathrm{i}^{-n} \\ & \times J_{n+1}(\xi') \sin\alpha (1-\mathrm{e}^{-\Delta/T_1^S}) \mathrm{e}^{\mathrm{i}\omega_S(\tau+t_2)} \\ & \times \mathrm{e}^{-(\tau+t_2)/T_2^S} \mathrm{e}^{-(b_1+b_2+b_5)D_T^S}, \end{aligned} \tag{1}$$

where $J_n(\xi)$ and $J_n(\xi')$ are the n-order Bessel functions; $b_1 = \gamma^2 G_1^2 \delta_1^2 (\Delta_1 - \delta_1/3)$ is the "active" diffusion weighting factor, in which Δ_1 is the time interval between the first pair of gradient pulses; $b_2 = \gamma^2 G^2 \delta_2^3/3$ is the diffusion weighting factor of the coherence-selection gradient immediately before the $(\beta)_y$ RF pulse; the diffusion weighting factors b_3 and b_5 are complex expressions depending on both the two gradients immediately before and after the $(\beta)_y$ RF pulse and the detection time t_2 , and the diffusion weighting factor $b_4 = n^2\gamma^2 G^2 \delta_2^2 (\delta_2/3 + t_2)$ is due to the gradient after the $(\beta)_y$ RF pulse and continuing diffusion decay during detection period t_2; $\xi' = 2\xi/3$ and $\xi = \gamma\mu_0 M_0^I \sin\alpha \sin\beta (1-\mathrm{e}^{-\Delta/T_1^I}) \mathrm{e}^{-\tau/T_2^I} \mathrm{e}^{-(b_1+b_2)D_T^I} [1-\mathrm{e}^{-(k^2 D_T^I + 1/T_1^I)t_2}] (k^2 D_T^I + 1/T_1^I)^{-1}$, in which $k = \gamma G \delta_2$ is the magnetization helix created by the gradient before the $(\beta)_y$ pulse.

When the $(\alpha)_y$ RF pulse is selective to the I spin and the $(\beta)_y$ pulse is non-selective (see Fig. 1), the resulting signal with a quadrature detection scheme is described by Eq. (9) in [19]:

$$\begin{aligned} M_+^{\text{total}}(\Delta+\tau+t_2) = {} & M_0^I \mathrm{i}^{-(n+1)} \left\{ \frac{nJ_n(\xi)}{\xi} - 0.5[J_{n-1}(\xi) \right. \\ & \left. - J_{n+1}(\xi)] \cos\beta \right\} \sin\alpha (1-\mathrm{e}^{-\Delta/T_1^I}) \\ & \times \mathrm{e}^{-(\tau+t_2)/T_2^I} \mathrm{e}^{-(b_1+b_2+b_3)D_T^I} \\ & + M_0^I \mathrm{i}^{-n+1} J_n(\xi) \\ & \times \sin\beta [\cos\alpha \mathrm{e}^{-\tau/T_1^I}(1-\mathrm{e}^{-\Delta/T_1^I}) \\ & + (1-\mathrm{e}^{-\tau/T_1^I})] \mathrm{e}^{-t_2/T_2^I} \mathrm{e}^{-b_4 D_T^I} \\ & + M_0^S \mathrm{i}^{-n+1} J_n(\xi') \sin\beta \\ & \times (1-\mathrm{e}^{-\Delta/T_1^S}) \mathrm{e}^{\mathrm{i}\omega_S t_2} \mathrm{e}^{-t_2/T_2^S} \mathrm{e}^{-b_4 D_T^S}. \end{aligned} \tag{2}$$

Eqs. (1) and (2) provide general analytical expressions for signals from different coherence orders selected by varying the ratio n of coherence-selection gradients. The first two terms in Eq. (1) represent the detectable signals of I spin, which is the same as the first two terms in Eq. (2). The first terms in Eqs. (1) and (2) include the conventional Hahn echo when $n = +1$ or anti-echo when $n = -1$ for I spin. When the diffusion and relaxation are neglected and the flip angle $\beta = \pi/2$, the observable signals of I spin are identical to the results reported previously [21–23]. The second terms in Eqs. (1) and (2) are the residual conventional SQC signal of I spin. The third terms in in Eqs. (1) and (2) provide the quantitative relationship between the experimental parameters and observed S signals originating from iMQCs. Since the properties of S signals are different from those of I signals, we will quantitatively investigate the properties of the S signals in the following discussion.

First, we discuss the experimental conditions corresponding to Eq. (1). Since the properties of S signals originating from $n = 0$ and $n = \pm 2$ iMQCs have been discussed in detail in our previous paper [25], here we will focus on the properties of S signals from the third-order spin interactions (i.e., three-spin orders) in the cases of $n = \pm 1$ and $n = \pm 3$. In the case of $n = -1$, the S signal in Eq. (1) can be written as:

$$\begin{aligned} M_+^S(\Delta+\tau+t_2) = {} & M_0^S \mathrm{i} J_0(\xi') \sin\alpha (1-\mathrm{e}^{-\Delta/T_1^S}) \\ & \times \mathrm{e}^{\mathrm{i}\omega_S(\tau+t_2)} \mathrm{e}^{-(\tau+t_2)/T_2^S} \mathrm{e}^{-(b_1+b_2+b_5)D_T^S}. \end{aligned} \tag{3}$$

Since the condition of small dipolar field effects, $\xi' \ll 1$, is safely satisfied under ordinary experimental situations [29], the Taylor expansion of the Bessel function results in $J_0(\xi') \approx 1 - \xi'^2/4$. Substituting the above-given relation into Eq. (3), we have

$$M_+^S(\Delta+\tau+t_2) = M_0^S \sin\alpha(1-\mathrm{e}^{-\Delta/T_1^S}) \times \mathrm{e}^{\mathrm{i}\omega_S(\tau+t_2)}\mathrm{e}^{-(\tau+t_2)/T_2^S}\mathrm{e}^{-(b_1+b_2+b_5)D_T^S} - \frac{1}{9}\xi^2 M_0^S \sin\alpha(1-\mathrm{e}^{-\Delta/T_1^S}) \times \mathrm{e}^{\mathrm{i}\omega_S(\tau+t_2)}\mathrm{e}^{-(\tau+t_2)/T_2^S}\mathrm{e}^{-(b_1+b_2+b_5)D_T^S}. \quad (4)$$

The first term in Eq. (4) is a gradient echo without dipolar field effects, and the second term is the S signal from iSQCs of the third-order spin interactions. Clearly, the small signal described by the second term in Eq. (4) is difficult to be selectively detected underneath the strong conventional SQC signal described by the first term. This phenomenon has been reported recently [21–23].

In the case of $n = +1$, Eq. (1) yields the following form after some algebra manipulations:

$$\begin{aligned} M_+^S(\Delta+\tau+t_2) &= M_0^S J_2(\xi')\sin\alpha(1-\mathrm{e}^{-\Delta/T_1^S})\mathrm{e}^{\mathrm{i}\omega_S(\tau+t_2)} \times \mathrm{e}^{-(\tau+t_2)/T_2^S}\mathrm{e}^{-(b_1+b_2+b_5)D_T^S} \\ &= \frac{1}{18}\xi^2 M_0^S \sin\alpha(1-\mathrm{e}^{-\Delta/T_1^S}) \times \mathrm{e}^{\mathrm{i}\omega_S(\tau+t_2)}\mathrm{e}^{-(\tau+t_2)/T_2^S}\mathrm{e}^{-(b_1+b_2+b_5)D_T^S} \\ &\propto \sin^3\alpha\sin^2\beta(1-\mathrm{e}^{-\Delta/T_1^I})^2(1-\mathrm{e}^{-\Delta/T_1^S}) \times \mathrm{e}^{-\tau(2/T_2^I+1/T_2^S)-t_2/T_2^S}\mathrm{e}^{-(b_1+b_2)(D_T^I+D_T^S)-b_5D_T^S}. \end{aligned} \quad (5)$$

Eq. (5) provides an analytical expression to quantify the S signal of $n = +1$ from the third-order spin interactions, which can be selectively detected from other coherence transfer paths. In the case of $n = -3$, Eq. (1) yields the following form after some algebra manipulations:

$$\begin{aligned} M_+^S(\Delta+\tau+t_2) &= M_0^S J_{-2}(\xi')\sin\alpha(1-\mathrm{e}^{-\Delta/T_1^S}) \times \mathrm{e}^{\mathrm{i}\omega_S(\tau+t_2)}\mathrm{e}^{-(\tau+t_2)/T_2^S}\mathrm{e}^{-(b_1+b_2+b_5)D_T^S} \\ &= \frac{1}{18}\xi^2 M_0^S \sin\alpha(1-\mathrm{e}^{-\Delta/T_1^S}) \times \mathrm{e}^{\mathrm{i}\omega_S(\tau+t_2)}\mathrm{e}^{-(\tau+t_2)/T_2^S}\mathrm{e}^{-(b_1+b_2+b_5)D_T^S} \\ &\propto \sin^3\alpha\sin^2\beta(1-\mathrm{e}^{-\Delta/T_1^I})^2(1-\mathrm{e}^{-\Delta/T_1^S}) \times \mathrm{e}^{-\tau(2/T_2^I+1/T_2^S)-t_2/T_2^S}\mathrm{e}^{-(b_1+b_2)(D_T^I+D_T^S)-b_5D_T^S}. \end{aligned} \quad (6)$$

Eq. (6) provides an analytical expression to quantify the S signal of $n = -3$ from the third-order spin interactions. It is the same expression as the $n = +1$ case, so it can be selectively detected, too.

In the case of $n = +3$, Eq. (1) yields the following form after some algebra manipulations:

$$\begin{aligned} M_+^S(\Delta+\tau+t_2) &= M_0^S J_4(\xi')\sin\alpha(1-\mathrm{e}^{-\Delta/T_1^S}) \times \mathrm{e}^{\mathrm{i}\omega_S(\tau+t_2)}\mathrm{e}^{-(\tau+t_2)/T_2^S}\mathrm{e}^{-(b_1+b_2+b_5)D_T^S} \\ &= \frac{1}{1944}\xi^4 M_0^S \sin\alpha(1-\mathrm{e}^{-\Delta/T_1^S}) \times \mathrm{e}^{\mathrm{i}\omega_S(\tau+t_2)}\mathrm{e}^{-(\tau+t_2)/T_2^S}\mathrm{e}^{-(b_1+b_2+b_5)D_T^S}. \end{aligned} \quad (7)$$

Eq. (7) suggests that the signal of $n = +3$ is too weak to be observed.

Now we discuss the experimental conditions corresponding to Eq. (2). In the cases of $n = \pm 2$, we have

$$\begin{aligned} M_+^S(\Delta+\tau+t_2) &= M_0^S J_2(\xi')\sin\beta(1-\mathrm{e}^{-\Delta/T_1^S}) \times \mathrm{e}^{\mathrm{i}\omega_S t_2}\mathrm{e}^{-t_2/T_2^S}\mathrm{e}^{-b_4D_T^S} \\ &= \frac{1}{18}\xi^2 M_0^S \sin\beta(1-\mathrm{e}^{-\Delta/T_1^S}) \times \mathrm{e}^{\mathrm{i}\omega_S t_2}\mathrm{e}^{-t_2/T_2^S}\mathrm{e}^{-b_4D_T^S} \\ &\propto \sin^2\alpha\sin^3\beta(1-\mathrm{e}^{-\Delta/T_1^I})^2(1-\mathrm{e}^{-\Delta/T_1^S}) \times \mathrm{e}^{-2\tau/T_2^I-t_2/T_2^S}\mathrm{e}^{-(b_1+b_2)(2D_T^I)-b_4D_T^S}. \end{aligned} \quad (8)$$

It suggests that the signal of $n = \pm 2$ from the third-order spin interactions can be selectively detected and has the same amplitude as that described by Eq. (5) when diffusion and relaxation processes are neglected.

In the case of $n = 0$, we have

$$\begin{aligned} M_+^S(\Delta+\tau+t_2) &= M_0^S J_0(\xi')\sin\beta(1-\mathrm{e}^{-\Delta/T_1^S}) \times \mathrm{e}^{\mathrm{i}\omega_S t_2}\mathrm{e}^{-t_2/T_2^S}\mathrm{e}^{-b_4D_T^S} \\ &= M_0^S \sin\beta(1-\mathrm{e}^{-\Delta/T_1^S})\mathrm{e}^{\mathrm{i}\omega_S t_2}\mathrm{e}^{-t_2/T_2^S} \times \mathrm{e}^{-b_4D_T^S} - \frac{1}{9}\xi^2 M_0^S \sin\beta(1-\mathrm{e}^{-\Delta/T_1^S}) \times \mathrm{e}^{\mathrm{i}\omega_S t_2}\mathrm{e}^{-t_2/T_2^S}\mathrm{e}^{-b_4D_T^S}. \end{aligned} \quad (9)$$

The first term in Eq. (9) is a conventional SQC signal, and the second term is the S signal from iZQC of the third-order spin interactions. Clearly, the small signal described by the second term is difficult to be selectively detected underneath the strong conventional SQC signal described by the first term. Our previous report has pointed out this phenomenon [19].

2.2. iMQC treatment

As a complementary method, iMQC treatment is employed to intuitively demonstrate that the S signals originate from intermolecular longitudinal three spin-orders. In what follows, we will focus only on the intermolecular longitudinal three-spin order, labeled as 1, 2, and 3. If the spins I and S stand for protons from different components of the mixture, let us consider a longitudinal three-spin order, $I_{1z}\,I_{2z}\,S_{3z}$, originating from higher-order expansion terms of the equilibrium density operator. For simplicity, the flip angles of α and β are set to $\pi/2$.

When the experimental conditions corresponding to Eq. (1) are employed, the term proportional to $I_{1z}I_{2z}S_{3z}$ in the equilibrium density operator is rotated into $I_{1x}I_{2x}S_{3x}$ by the first $\pi/2$ pulse. Due to small residual dipolar coupling and short evolution period τ, the residual dipolar interaction is unimportant during τ. The term $I_{1x}I_{2x}S_{3x}$ can be rewritten as a combination of

SQCs and triple-quantum coherences (TQCs) which evolve at four different frequencies during the evolution period:

$$\begin{aligned} I_{1z}I_{2z}S_{3z} \xrightarrow{(\pi/2)_y} I_{1x}I_{2x}S_{3x} = \frac{1}{8}(&I_1^+I_2^+S_3^+ + I_1^+I_2^+S_3^- \\ &+ I_1^+I_2^-S^+ + I_1^-I_2^+S_3^+ \\ &+ I_1^+I_2^-S_3^- + I_1^-I_2^+S_3^- \\ &+ I_1^-I_2^-S_3^+ + I_1^-I_2^-S_3^-). \end{aligned} \tag{10}$$

There are six triple-spin SQC terms and two triple-spin TQC terms in Eq. (10). Since only density operator components with coherence order $p = -1$ in the final density operator can contribute to the observable signal [30], all components with coherence order $p \neq -1$ can be disregarded. After the second $\pi/2$ pulse, which is selective to spin I is applied, the term $I_1^+I_2^+S_3^-$ for $n = +1$, the two terms $I_1^-I_2^+S_3^-$ and $I_1^+I_2^-S_3^-$ for $n = -1$, and the term $I_1^-I_2^-S_3^-$ for $n = -3$ can be converted to the potential observable coherence term $I_{1z}I_{2z}S_3^-$, which requires two dipolar couplings to generate the observable S^- signal. However, all S_3^+ terms are impossible to be converted to the observable S^- signal by the selective $\pi/2$ pulse and the following evolution process. The longitudinal three-spin order, $8I_{1z}I_{2z}S_{3z}$, converts into a potential observable term, $I_{1z}I_{2z}S_3^-$, through the following pathways:

$$\begin{aligned} &8I_{1z}I_{2z}S_{3z} \xrightarrow{(\pi/2)_y} 8I_{1x}I_{2x}S_{3x} \\ &= \begin{cases} I_1^-I_2^-S_3^- & \xrightarrow{(\pi/2)_y^I+(1:-3)\text{ gradient ratio}} I_{1z}I_{2z}S_3^- \\ I_1^+I_2^-S_3^- + I_1^-I_2^+S_3^- & \xrightarrow{(\pi/2)_y^I+(1:-1)\text{ gradient ratio}} 2I_{1z}I_{2z}S_3^- \\ I_1^+I_2^+S_3^- & \xrightarrow{(\pi/2)_y^I+(1:+1)\text{ gradient ratio}} I_{1z}I_{2z}S_3^- \\ \text{including } S_3^+\text{terms} & \xrightarrow{(\pi/2)_y^I+(1:n)\text{ gradient ratio}} \text{No signal} \end{cases} \end{aligned} \tag{11}$$

A similar analysis can be carried out for experimental conditions corresponding to Eq. (2). We shall not go through detailed analysis. The coherence paths can be sketched as follows:

$$\begin{aligned} &8I_{1z}I_{2z}S_{3z} \xrightarrow{(\pi/2)_y^I} 8I_{1x}I_{2x}S_{3z} \\ &= \begin{cases} 2I_1^-I_2^-S_z & \xrightarrow{(\pi/2)_y+(1:-2)\text{ gradient ratio}} I_{1z}I_{2z}S^- \\ 2(I_1^+I_2^- + I_1^-I_2^+)S_z & \xrightarrow{(\pi/2)_y+(1:0)\text{ gradient ratio}} 2I_{1z}I_{2z}S^- \\ 2I_1^+I_2^+S_z & \xrightarrow{(\pi/2)_y+(1:+2)\text{ gradient ratio}} I_{1z}I_{2z}S^- \end{cases} \end{aligned} \tag{12}$$

Eq. (12) shows that the signals of a three-spin order in the cases of $n = \pm 2$ have the same efficiency as the cases of $n = +1$ and $n = -3$ in Eq. (11), which are also the same as those described in Eqs. (5) and (6) using the dipolar field treatment. The efficiency in the cases of $n = -1$ in Eq. (11) and $n = 0$ in Eq. (12) seems to be high, but these signals cannot be selected from the strong conventional SQC signals as described in Eqs. (4) and (9). In contrast to the dipolar field treatment which provides completely quantitative predictions, the iMQC treatment given here provides quantitative relations between observables in similar multi-quantum experiments, not quantitative predictions about the actual magnitude of each observed signal.

3. Experimental

All experiments were carried out at 298 K using a Varian Unity plus 500 MHz spectrometer equipped with self-shielded z-gradient coils and a 5 mm HCN triple-resonance RF coil of 1.5 cm effective length. A two-component sample of benzene (C_6H_6) and acetone (CH_3COCH_3) was used. About 30% (by volume) acetone-d_6 was added to the sample for field lock and shimming of the spectrometer as well as for reducing radiation damping effects. The diffusion weighting gradients had amplitude $G_1 = 0.065$ T/m and duration $\delta_1 = 2$ ms, and the coherence-selection gradient had amplitude $G = 0.065$ T/m and duration $\delta_2 = 2$ ms. $\pi/2$ pulse width of a RF hard pulse was extended from 6 to 140 μs by detuning the probe to further suppress the radiation damping during the evolution and detection periods. $\pi/2$ Gaussian pulse had the pulse width of 4 ms. Acquisition time was 1.5 s, and a long pulse repetition time of 50 s was applied to avoid the possibility of stimulated echoes.

4. Results and discussion

4.1. Relative signal intensities

To compare the relative signal intensities of different coherence orders from intermolecular three-spin orders, several typical spectra were acquired under different conditions. The conventional 1D spectrum is shown in Fig. 2A. The flip angles of α and β were set to $\pi/2$. When the β RF pulse was used to selectively excite the benzene peak (I spin), the spectra shown in Figs. 2B–E correspond to the signals in the cases of $n = -1$, $+1$, -3, and $+3$, respectively. Since the conventional anti-echo for I spin and gradient echo for S spin were formed by the $n = -1$ coherence-selection gradients, both the S and I signals as shown in Fig. 2B are very strong. In the case of $n = +1$, Fig. 2C shows a strong Hahn echo for I spin predicted by the first term in Eq. (1) and a weak S signal predicted by Eq. (5). It provides a convenient way to separate the weak iSQC signal of S spin from the strong Hahn echo of I spin. It is the first time to successfully separate the pure iSQC originating from homonuclear three-spin orders. In the case of $n = -3$,

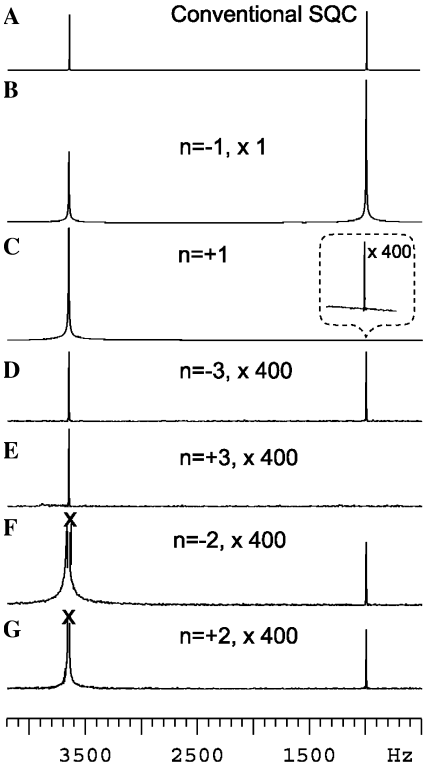

Fig. 2. Signals from different coherence orders. (A) Single-pulse ^{1}H phase-sensitive spectrum of a mixture of benzene (left) and acetone (right). When the experimental conditions corresponding to Eq. (1) were employed, (B) $n = -1$, (C) $n = +1$, (D) $n = -3$, and (E) $n = +3$. When the experimental conditions corresponding to Eq. (2) were employed, (F) $n = -2$ and (G) $n = +2$. Data inside the box are amplificatory times.

Fig. 2D shows that the S signal as predicted by Eq. (6) and the I signal originate from intermolecular three-spin orders. In the case of $n = +3$, Fig. 2E shows that only the I signal originating from intermolecular three-spin operators is observed. Such peculiar a feature can be explained by Eq. (7). When the α RF pulse was applied to selectively excite the ^{1}H signal of benzene (I spin), the signals of I and S spins originating from $n = +2$ and $n = -2$ coherence orders are shown in Figs. 2F and G, respectively. The signals of I spin are mainly from two-spin terms, i.e., the second-order spin interactions, which have been discussed in most literature [4,25]. However, the signals of S spin from iDQCs predicted by Eq. (8) are from three-spin terms, i.e., the third-order spin interactions, which have not been discussed in literature yet. Our theoretical and experimental results indicated that the S signals from iDQC of three-spin orders (Figs. 2F and G) almost have equal intensity as those from iSQC (Fig. 2B) or iTQC (Fig. 2D) of three-spin orders. Although the relative signal intensities of S spin with different coherence orders may be quite different, all experimental results mentioned above are in agreement with the theoretical predictions.

Now we discuss the relative signal intensity between the iSQC and convention SQC. In the case of $n = -1$, the first term in Eq. (4) is a gradient echo, so the strong S signal as shown in Fig. 2B is almost equal to the conventional SQC signal under the same experimental conditions. In the case of $n = +1$, the iSQC signal originating from intermolecular homonuclear three-spin orders is shown in Fig. 2C. The magnitude of S signal from iSQC is about 800 times weaker than that of the conventional S signal. Since the pure iSQC signal originating from homonuclear three-spin orders is much smaller than the conventional SQC signal, it is difficult to characterize the properties of iSQC signals from intermolecular three-spin orders when the iSQC and conventional SQC signals overlap [21–23]. In principle, the experimental results can be compared with the corresponding theoretical predictions from Eqs. (4) and (5). However, Eq. (5) includes complex diffusion and relaxation processes which compete with the action of the dipolar field. A quantitative analysis of the problems will be given elsewhere in a separated paper.

4.2. Optimal RF flip angles

Since the S signals may be selectively detected, the quantitative relationship between the relative signal intensities and optimized flip angles can be investigated using the flip angles α and β as independent variables. The relative intensities of S signals described by Eqs. (5) and (6) are simplified as

$$f_S(\alpha,\beta) \propto \sin^3\alpha \sin^2\beta \quad (n = +1 \text{ or } -3). \tag{13}$$

Similarly, the relative intensity of S signals described by Eq. (8) is simplified as

$$f_S(\alpha,\beta) \propto \sin^2\alpha \sin^3\beta \quad (n = +2 \text{ or } -2). \tag{14}$$

Eqs. (13) and (14) suggest that both optimal RF flip angles of α and β for S signals are $\pi/2$, but their relationships between relative intensity and flip angles are different. The former is directly proportional to $\sin^3\alpha \sin^2\beta$ while the latter is directly proportional to $\sin^2\alpha \sin^3\beta$. To verify the theoretical predictions, the dependence of normalized signals on RF flip angles α and β was measured. The pre-saturation unit and the "active" diffusion weighting module were set to zero. The relative signal intensities of acetone (S spin) from three-spin orders were measured as a function of flip angles with α or β varied from 0° to 180°. A fixed evolution time $\tau = 3$ ms was used, to minimize signal attenuation due to transverse relaxation during the evolution period. In Fig. 3, normalized theoretical curves based on Eqs. (13) and (14) are plotted as a function of α or β together with experimental observations. For comparison, normalized theoretical curves $\sin\alpha$ and $\sin\beta$ were also plotted as a function of flip angles. Experimental results showed that both the relative signal intensities and the optimal flip

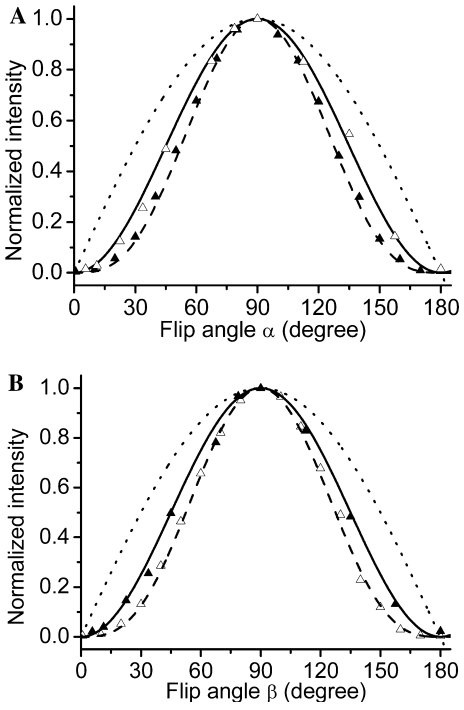

Fig. 3. Normalized signal intensities from intermolecular three-spin orders are plotted as a function of the flip angles. The sample is a mixture of benzene and acetone, in which benzene was selectively excited. The symbol "▲" indicates experimental observations of the ^{1}H signal of acetone with the conditions corresponding to Eq. (5), and the solid line is its normalized theoretical curve, $\sin^3\alpha \sin^2\beta$. The symbol "Δ" indicates experimental observations with the conditions corresponding to Eq. (8), and the dashed line is its theoretical curve, $\sin^2\alpha \sin^3\beta$. The dashed-dotted line is the theoretical curve of $\sin\alpha\sin\beta$function. (A) varying flip angle α with $\beta = \pi/2$ and (B) varying flip angle β with $\alpha = \pi/2$.

angles of α and β for the S signals from three-spin orders are in excellent agreement with the theoretical predictions.

4.3. Longitudinal relaxation

The S signals originating from iSQCs of three-spin orders are dependent on the recovery period Δ of magnetization from pre-saturation. The analytical expression described by Eq. (5) predicts that S signals follow a specific relaxation relationship. The longitudinal relaxation times of ^{1}H NMR signals in a mixture of benzene and acetone were measured by the conventional saturation-recovery method. Experimental data of normalized integrated amplitudes with Δ varied from 0.5 to 35 s were used to estimate the longitudinal relaxation time. The longitudinal relaxation times from best-fit based on the mono-exponential function $(1 - e^{-\Delta/T_1})$ are $T_1^I = 8.14 \pm 0.8$ s for benzene and $T_1^S = 7.03 \pm 0.8$ s for acetone. When I and S spins were saturated simultaneously and the ^{1}H signal of benzene was selectively excited by the $(\beta)_y$ RF pulse, the experimental observations of the ^{1}H signal of acetone were indicated by the symbols "▲".

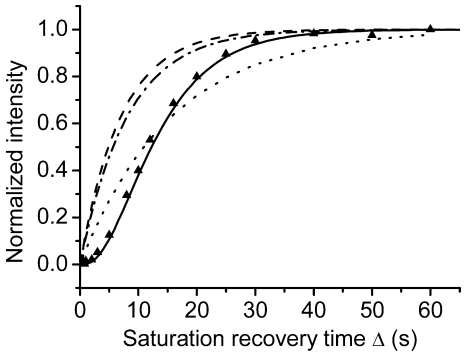

Fig. 4. Normalized signal intensities due to longitudinal relaxation process are plotted as functions of the saturation recovery time Δ with the experimental conditions corresponding to Eq. (5). For a mixture of benzene and acetone, the conventional SQC longitudinal relaxation times of the ^{1}H signals of benzene and acetone were found to be 8.14 and 7.03 s, respectively. The symbols "▲" indicate experimental observations of the ^{1}H signal of acetone when the ^{1}H signals of benzene and acetone are saturated simultaneously. The solid line is fitted using the theoretical expression $(1 - e^{-\Delta/T_1^I})^2 (1 - e^{-\Delta/T_1^S})$ with $T_1^I = 8.14$ s and $T_1^S = 7.03$ s, the dash-dot line is fitted using the expression $(1 - e^{-\Delta/T_1^I})$ with $T_1^I = 8.14$ s, the dash line is fitted using the expression $(1 - e^{-\Delta/T_1^S})$ with $T_1^S = 7.03$ s, and the dot line is fitted using a mono-exponential expression $(1 - e^{-\Delta/T_1})$, resulting in $T_1 = 15.8$ s.

Data for $n = +1$ longitudinal relaxation process of ^{1}H signal of acetone, together with fitting of different functions are shown in Fig. 4. The solid line is fitted using the theoretical expression $(1 - e^{-\Delta/T_1^I})^2 (1 - e^{-\Delta/T_1^S})$ with $T_1^I = 8.14$ s and $T_1^S = 7.03$ s, the dash dot line is fitted using the expression $(1 - e^{-\Delta/T_1^I})$ with $T_1^I = 8.14$ s, the dash line is fitted using the expression $(1 - e^{-\Delta/T_1^S})$ with $T_1^S = 7.03$ s, and the dot line is fitted using a mono-exponential expression $(1 - e^{-\Delta/T_1})$, resulting in $T_1 = 15.8$ s. It demonstrates that the experimental observations are in good agreement with the multiple-exponential relaxation relationship, $(1 - e^{-\Delta/T_1^I})^2 (1 - e^{-\Delta/T_1^S})$, predicted by Eq. (5). This unusual longitudinal relaxation behavior can be explained as follows: the simultaneous pre-saturation RF pulse reduces the initial I and S magnetization by an amount of $(1 - e^{-\Delta/T_1^I})$ and $(1 - e^{-\Delta/T_1^S})$, respectively; the S signal of iSQC originates from three-spin order term, $I_{1z}I_{2z}S_{3z}$, so the longitudinal relaxation behavior of the S signal for $n = +1$ follows the relationships, $(1 - e^{-\Delta/T_1^I})^2 (1 - e^{-\Delta/T_1^S})$.

4.4. Diffusion properties

Apparent diffusion coefficients, $D^S_{T,\mathrm{app}}$, of S signals in different coherence orders during the evolution period are predicted by Eqs. (5), (6), and (8). A series of diffusion measurements were performed in order to verify the predictive power. The experiments were carried out for an appropriate set of gradient amplitude G_1 values so that the signal decay due to diffusion can be monitored. First, the conventional SQC diffusions of benzene and acetone were measured according to the gradient echo sequence

and the self-diffusion coefficients of the mixture were yielded: $D_T^I = (3.88 \pm 0.01) \times 10^{-9}\ \mathrm{m^{-2}\,s}$ for benzene and $D_T^S = (5.20 \pm 0.01) \times 10^{-9}\ \mathrm{m^{-2}\,s}$ for acetone. Experimental results are displayed in Fig. 5. Experimental data were fitted against the function derived theoretically in the previous section. When the experimental conditions corresponding to Eqs. (5) and (6) were employed, the fitted apparent diffusion ratios for S signal are $D^S_{T,\mathrm{iSQC}} = (12.59 \pm 0.12) \times 10^{-9} \approx 2D_T^I + D_T^S$ for $n = +1$ and $D^S_{T,\mathrm{iTQC}} = (12.63 \pm 0.15) \times 10^{-9} \approx 2D_T^I + D_T^S$ for $n = -3$. Since the experimental data of $n = -3$ almost overlap those of $n = +1$, the data of $n = -3$ are not shown in Fig. 5. When the experimental conditions corresponding to Eq. (8) ($n = +2$) were employed, the fitted apparent diffusion ratio for S signal is $D^S_{T,\mathrm{iDQC}} = (7.61 \pm 0.08) \times 10^{-9} \approx 2D_T^I$. These results are in excellent agreement with our theoretical predictions.

In addition, Eqs. (5) and (6) also predict that apparent transverse relaxation time, $T^S_{2,\mathrm{app}}$, of S spin from three-spin orders for $n = +1$ and $n = -3$ during the evolution period follows the relationship $1/T^S_{2,\mathrm{app}} = 2/T_2^I + 1/T_2^S$, which is similar to the theoretical results in a single-component three-spin system reported by Warren et al. [23]. However, Eq. (8) predicts that apparent transverse relaxation time of S spin from three-spin orders for $n = \pm 2$ during the evolution period follows the relationship $1/T^S_{2,\mathrm{app}} = 2/T_2^I$. On the other hand, methods for efficiently exciting multiple-quantum coherence are central building blocks in iMQC experiments. For a two-component mixture in which one component only bears a single spin 1/2 of type I and the other only bears a single spin 1/2 of type S, the long-range intermolecular dipolar interactions between I and S spins are very weak. From the viewpoint of selective excitation, I and S spins can be thought of as isolated spin systems. It makes selective excitation easy to accomplish. The theoretical predictions and experimental results demonstrated that selective excitations are suitable for efficient acquisition of signals from intermolecular multiple-spin orders. These results confirm the validity of the theoretical developments given in the previous section.

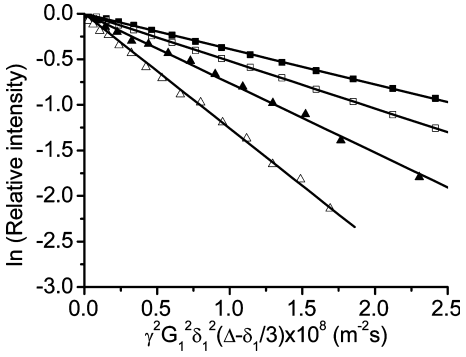

Fig. 5. Measurements of apparent diffusion rates of a mixture of benzene (I spin) and acetone (S spin) G_1 was used as independent variable to control signal attenuation, and natural logarithms of the signal intensity versus $b_1 = \gamma^2 G_1^2 \delta_1^2 (\Delta_1 - \delta_1/3)$ are plotted. The symbol "■" stands for the experimental data of conventional SQC diffusion decay for I component, "□" for S component due to conventional SQC diffusion, "▲" for S component with the experimental conditions corresponding to Eq. (8), and "△" for S component with the experimental conditions corresponding to Eq. (5). Solid lines are best fits to the experimental data. The apparent diffusion rates calculated from the slope of the best fitting are 3.88, 5.20, 7.61, and $12.59 \times 10^{-9}\ \mathrm{m^2\,s^{-1}}$, respectively.

5. Conclusions

In this paper, different signals originate from homonuclear intermolecular three-spin terms in the equilibrium density matrix were analyzed by dipolar field and iMQC treatments. Valuable insights about diffusion and relaxation features from intermolecular three-spin orders are obtained from the analytical expressions. Dependence of the signals of three-spin orders on flip angles can be predicted by the analytical expressions. Even though detection of the signals from three-spin operators may be hampered by the strong conventional SQC signals in the past, it has been demonstrated in the present paper, that selective excitation and two-component spin system can be employed to separate the different NMR signals (including weak iSQC signals) from the strong conventional SQC signals. For the first time, the weak iSQC signals from three-spin orders was separated and characterized experimentally. We showed that 3-spin n-quantum coherences ($n = +1$, ± 2, and -3) are effectively separated from other coherences. These novel homonuclear techniques based on intermolecular "third-order" dipolar interactions appear to be complementary to the existing iMQC methodology based on "second-order" dipolar interactions. The theoretical predictions of diffusion and relaxation properties of the signals from the three-spin orders are verified and characterized in detail. All experimental observations are in excellent agreement with the theoretical predictions. Since the signals from three-spin orders are usually much smaller than those from two-spin orders, it seems that the signals from three-spin orders are difficult to find general utility. However, our experimental scheme based on a two-component sample with selective RF pulses supplies a convenient way to understand the pronounced mechanism of the different signals from longitudinal three-spin orders. Moreover, the selective excitation concept in iMQCs may prove useful in other fields such as the high-resolution NMR spectra in inhomogeneous fields via intermolecular dipolar field.

Acknowledgments

This work was partially funded by the NNSF of China under Grants 10234070 and 10375049, the NSF of

Fujian under Grant A0210003, and the program for Promoting Academic Excellence of Universities of Taiwan.

References

[1] G. Deville, M. Bernier, J.M. Delrieux, NMR multiple echoes observed in solid ^{3}He, Phys. Rev. B 19 (1979) 5666–5688.
[2] R. Bowtell, R.M. Bowley, P. Glover, Multiple spin echoes in liquid in a high magnetic-field, J. Magn. Reson. J. Magn. Reson. 88 (1990) 643–651.
[3] J. Jeener, Collective effects in liquid NMR: dipolar field and radiation damping, in: D.M. Grant, R.K. Harris (Eds.), Encyclopedia of Nuclear Magnetic Resonance, vol. 9, Wiley, New York, 2002, pp. 642–679.
[4] W.S. Warren, W. Richter, A.H. Andreotti, B.T. Farmer II, Generation of impossible cross-peaks between bulk water and biomolecules in solution NMR, Science 262 (1993) 2005–2009.
[5] S. Lee, W. Richter, S. Vathyam, W.S. Warren, Quantum treatment of the effects of dipole–dipole interactions in liquid nuclear magnetic resonance, J. Chem. Phys. 105 (1996) 874–900.
[6] J. Jeener, Equivalence between the "classical" and the "Warren" approaches for the effects of long range dipolar couplings in liquid nuclear magnetic resonance, J. Chem. Phys. 112 (2000) 5091–5094.
[7] R. Bowtell, P. Robyr, Structural investigations with the dipolar demagnetizing field in solution NMR, Phys. Rev. Lett. 76 (1996) 4971–4974.
[8] R. Bowtell, S. Gutteridge, C. Ramanathan, Imaging the long-range dipolar field in structured liquid state samples, J. Magn. Reson. 150 (2001) 147–155.
[9] S. Gutteridge, C. Ramanathan, R. Bowtell, Mapping the absolute value of M_0 using dipolar field effects, Magn. Reson. Med. 47 (2002) 871–879.
[10] Y.Y. Lin, S. Ahn, N. Murali, W. Brey, C.R. Bowers, W.S. Warren, High-resolution, >1 GHz NMR in unstable magnetic fields, Phys. Rev. Lett. 85 (2000) 3732–3735.
[11] Y.Y. Lin, N. Lisitza, S. Ahn, W.S. Warren, Resurrection of crushed magnetization and chaotic dynamics in solution NMR spectroscopy, Science 290 (2000) 118–121.
[12] S.Y. Huang, Y.Y. Lin, N. Lisitza, W.S. Warren, Signal interferences from turbulent spin dynamics in solution nuclear magnetic resonance spectroscopy, J. Chem. Phys. 116 (2002) 10325–10337.
[13] S. Capuani, R.T. Branca, A. Alesiani, B. Maraviglia, Intermolecular double-quantum NMR techniques to probe microstructures on porous media, Magn. Reson. Imag. 21 (2003) 413–414.
[14] F.M. Alessandri, S. Capuani, B. Maraviglia, Multiple spin echoes in heterogeneous systems: physical origins of the observed dips, J. Magn. Reson. 156 (2002) 72–78.
[15] W.S. Warren, S. Ahn, M. Mescher, M. Garwood, K. Ugurbil, W. Richter, R.R. Rizi, J. Hopkins, J.S. Leigh, MR imaging contrast enhancement based on intermolecular zero quantum coherences, Science 281 (1998) 247–251.
[16] J.H. Zhong, Z. Chen, E. Kwok, In vivo intermolecular double-quantum imaging on a clinical 1.5 T MR scanner, Magn. Reson. Med. 43 (2000) 335–341.
[17] Z. Chen, Z.W. Chen, J.H. Zhong, High-resolution NMR spectra in inhomogeneous fields via IDEAL (intermolecular dipolar-interaction enhanced all lines) method, J. Am. Chem. Soc. 126 (2004) 446–447.
[18] S. Capuani, F. Curzi, F.M. Alessandri, B. Maraviglia, A. Bifone, Characterization of trabecular bone by dipolar demagnetizing field MRI, Magn. Reson. Med. 46 (2001) 683–689.
[19] Z. Chen, Z.W. Chen, J.H. Zhong, Observation and characterization of intermolecular homonuclear single-quantum coherences in liquid nuclear magnetic resonance, J. Chem. Phys. 117 (2002) 8426–8435.
[20] S. Ahn, W.S. Warren, Effects of intermolecular dipolar couplings in solution NMR in separated time intervals: the competition for coherence transfer pathways, Chem. Phys. Lett. (1998) 121–129.
[21] I. Ardelean, R. Kimmich, Demagnetizing field effects on the Hahn echo, (vol 320, p. 81, 2000) Chem. Phys. Lett. 332 (2000) 624–625.
[22] I. Ardelean, R. Kimmich, Demagnetizing field effects on the Hahn echo, Chem. Phys. Lett. 320 (2000) 81–86.
[23] W.S. Warren, S.Y. Huang, S. Ahn, Y.Y. Lin, Understanding third-order dipolar effects in solution nuclear magnetic resonance: Hahn echo decays and intermolecular triple-quantum coherences, J. Chem. Phys. 116 (2002) 2075–2084.
[24] W.S. Warren, D.P. Weitekamp, A. Pines, High-order selective sequences in multiple-quantum NMR, J. Magn. Reson. 40 (1980) 581–583.
[25] Z. Chen, Z.W. Chen, J.H. Zhong, Quantitative characterization of intermolecular dipolar interactions of two-component systems in solution nuclear magnetic resonance, J. Chem. Phys. 115 (2001) 10769–10779.
[26] Z. Chen, J.H. Zhong, Unconventional diffusion behaviors of intermolecular multiple-quantum coherences in nuclear magnetic resonance, J. Chem. Phys. 114 (2001) 5642–5653.
[27] Z. Chen, G.X. Lin, J.H. Zhong, Diffusion of intermolecular zero- and double-quantum coherences in two-component spin systems, Chem. Phys. Lett. 333 (2001) 96–102.
[28] Z. Chen, Z.W. Chen, J.H. Zhong, Quantitative study of longitudinal relaxation related to intermolecular dipolar interactions in solution NMR, Chem. Phys. Lett. 333 (2001) 126–132.
[29] C. Ramanathan, R. Bowtell, Dynamics of the nuclear magnetic resonance COSY-revamped by asymmetric z-gradients (CRAZED) experiment, J. Chem. Phys. 114 (2001) 10854–10859.
[30] R.R. Ernst, G. Bodenhausen, A. Wokaun, Principles of Nuclear Magnetic Resonance in One and Two Dimensions, Clarendon Press, Oxford, 1987.